PLOS ONE

RESEARCH ARTICLE

LVRT capability enhancement of DFIG based wind turbine with coordination control of dynamic voltage restorer and inductive fault current limiter

Dongyin Zhang[1], **Hanping Xu**[1], **Li Qiao**[1], **Lei Chen**[2]*

1 State Grid Hubei Electric Power Company Limited Economic Research Institute, Wuhan, China, **2** School of Electrical Engineering and Automation, Wuhan University, Wuhan, China

* chen_lei@whu.edu.cn

Citation: Zhang D, Xu H, Qiao L, Chen L (2019) LVRT capability enhancement of DFIG based wind turbine with coordination control of dynamic voltage restorer and inductive fault current limiter. PLoS ONE 14(8): e0221410. https://doi.org/10.1371/journal.pone.0221410

Editor: Wei Yao, Huazhong University of Science and Technology, CHINA

Received: April 22, 2019

Accepted: August 6, 2019

Published: August 27, 2019

Data Availability Statement: All relevant data are within the paper, its Supporting Information files, and Figshare: Zhang, Dongyin; Xu, Hanping; Qiao, Li; Chen, Lei (2019): LVRT Capability Enhancement of DFIG based Wind Turbine with Coordination Control of Dynamic Voltage Restorer and Inductive Fault Current Limiter. figshare. Figure. https://doi.org/10.6084/m9.figshare.8557562.v1.

Funding: This work was supported by the National Natural Science Foundation of China (51507117), and the Fundamental Research Funds for the

Abstract

According to the coordination control of a dynamic voltage restorer (DVR) and an inductive fault current limiter (FCL), this paper proposes an efficient low-voltage ride-through (LVRT) scheme for a doubly fed induction generator (DFIG) based wind turbine. The DVR is located to the DFIG's stator circuit for stabilizing the terminal voltage and decreasing the generator current. The inductive FCL is connected to the DFIG's rotor circuit for suppressing the rotor overcurrent and protecting the converter. Theoretical discussions on structure, principle and scale criterion of the combined DVR-FCL are conducted, and simulation analyses of the proposed approach to handle symmetrical and asymmetrical faults are done in MATLAB/Simulink. In this study, the dynamic characteristics of the DFIG during the faults are analyzed from multiple aspects, and a detailed comparison of the proposed approach and the single action of DVR or FCL is carried out. From the simulation results, the effectiveness and superiority of the proposed approach are well demonstrated.

1 Introduction

In recent years, the contradiction between the increase of energy demands and the shortage of fossil fuels has been more and more serious, and to achieve sustainable socio-economic development, promoting the penetration of renewable energy (RE) in power systems has been regarded as a critical solution [1–3]. In a sense, to construct a smart energy city, the application of micro-grids can contribute to accommodating more various RE sources and decreasing their adverse effects caused by uncertainties [4]. As a representative of RE, wind energy has obtained the fastest growth, and the cumulative installed capacity of wind power generators all over the world may be more than 800 GW by 2021 [5,6].

Note that, energy quality is a significant feature to affect the stability and security of electric power systems, and it is very crucial to stabilize wind power generators under short-circuit faults. Wind turbines (WTs) should keep the grid-connected status for a certain time, and

Central Universities (2042018kf0214). State Grid Hubei Electric Power Company Limited Economic Research Institute, provided support in the form of salaries for authors DZ, HX, and LQ, but did not have any additional role in the study design, data collection and analysis, decision to publish, or preparation of the manuscript. The specific roles of these authors are articulated in the 'author contributions' section.

Competing interests: The authors declare that there are no conflicts of interest. DZ, HX, and LQ are employees of State Grid Hubei Electric Power Company Limited Economic Research Institute. There are no patents, products in development or marketed products to declare. This does not alter our adherence to PLOS ONE policies on sharing data and materials.

Abbreviations: 0, Initial time; *cs*, Controllable switch; ct1, Primary coil of coupling transformer; ct2, Secondary coil of coupling transformer; DC, Direct current; DFIG, Doubly fed induction generator; DVR, Dynamic voltage restorer; *e*, Electromagnetic force [V]; *f*, Fault; FCL, Fault current limiter; GSC, Generator side converter; *i*, Current [A]; *k*, Coupling factor [-]; *L*, Inductance [H]; LVRT, Low-voltage ride-through; *m*, Mutual; *Max*, Maximum; MPPT, Maximum power point tracking; *R*, Resistance [Ω]; *r*, Rotor; RE, Renewable energy; *ref*, Reference; RMS, Root-mean-square; RSC, Rotor side converter; *s*, Stator; SMES, Superconducting magnetic energy storage; *sys*, System; *V*, Voltage [V]; WT, Wind turbine; *X*, Reactance [Ω]; *Z*, Impedance [Ω]; *σ*, Leakage; *Ψ*, Flux [T]; *ω*, Angular velocity [rad/s].

this condition depends on the severity of faults or level of voltage sags to meet specific code demands, so called as low-voltage ride-through (LVRT) operation.

As the most widely WT, doubly fed induction generator (DFIG) has obtained considerable attention, and many different measures regarding the LVRT enhancement of DFIG have been suggested. Generally, the existing methods are classified as software and hardware approaches. The software solution is regarding an improved or updated control strategy with less cost, but it is just suitable for handling moderate fault conditions [7]. The hardware solution is to apply one or more devices with cost investment, and it has a good ability to deal with serious short-circuit faults. The literature review is presented as follows.

1.1 Literature review

In [8], an advanced current tracking controller is applied in the rotor-side converter (RSC). Scholars discuss how to determine a proper tracking coefficient for the controller, and the results show the transient fluctuations in the RSC can be well constrained. In [9], an available (generator side converter) GSC voltage is utilized to conduct the voltage compensation, and the DFIG's transient flux is controlled to obtain a desirable fault current limitation. In [10], a linear-quadratic regulator is implemented in the DFIG. This regulator serves as the supplementary control to prevent converter saturation. In [11], an optimal hierarchical control structure is proposed. The primary and secondary control levels are designed, and it is found that active and reactive power oscillations in the generator can be favorably mitigated. In [12,13], two improved controllers basing fuzzy logic are used in the RSC, and the key functions of the proposed controllers are to decrease the rotor current and inhibit the DC-link voltage. In [14], scholars investigate an analytical method to determine the control parameters of the DFIG subject to the capacity limit of the RSC. On the whole, the transient stability support from the software solutions towards the DFIG may be relatively moderate, and the improvements of optimizing current reference and introducing over-modulation could be appreciatively done.

In the following, the hardware solutions based on chopper circuit, voltage compensator/restorer and FCL are reviewed. In [15], the efficacy of a DC-link chopper on diminishing the DC overvoltage is validated, nevertheless it fails to assist the demagnetization of the electrical machine post-fault. In [16], scholars propose a modified DC chopper that can be inserted in a DFIG basing series or parallel connection. Although the modified structure makes certain improvements, the rotor current is still around its safety limit (2.0 pu). In [17], a minimised series voltage compensator is applied. Since the stator flux is well controlled, the generator is allowed to ride-through the grid disturbances.

In [18,19], scholars prove that a DVR is better than a crowbar circuit to handle the transient fluctuations of a DFIG. When the DVR is to solve serious voltage decline with a longer duration, it is needed to consider sufficient energy support [20]. To deeply explore the potentials of the DVR, an enhanced voltage control basing the combination of feed-forward and feedback is proposed in [21], and an improved topological structure is discussed in [22]. Using the DVR can offer flexible transient- and steady-state response for the DFIG. On the premise of meeting the DFIG's LVRT capability, it is recommended to reduce the DVR rating for making the solution be more practical. From this perspective, introducing a device with better economic performance to decrease the DVR rating might be an appropriate option.

Regarding the application of a FCL in a DFIG, studies focus on bridge-type [23–26] and superconducting-type FCLs [27–34]. In [23], a bridge-type FCL with bypass resistor is applied in a DFIG. The research results confirm its positive effects on reducing the flux and electromagnetic torque oscillations. In [24], the efficacy comparison of a bridge-type FCL and a series

dynamic braking resistor is carried out. It is illustrated that the FCL owns better suitability than the braking resistor in stabilizing a DFIG. In [25], a nonlinear control-based modified bridge-type FCL is presented. Owing to the structure improvement, the proposed FCL outperforms the conventional bridge-type FCLs to support the LVRT operation and has quicker withdrawal action. In [26], scholars propose a capacitive bridge-type FCL to increase the grid-side voltage, and a discharging resistor is configured to dissipate excess power for protecting the RSC.

In [27,28], an active-type SFCL and a flux-coupling-type SFCL are installed at the stator of a DFIG, and the two SFCLs both appear hybrid current-limiting impedance to suppress the transient fluctuations. Although an effective reduction in the stator current is realized, there is room for mitigating the rotor current. In [29–32], the contributions of the resistive SFCL in the DFIG rotor are evaluated. The stability of the RSC is strengthened, and the DC-link overvoltage is clearly alleviated. However, it is not good at enhancing the terminal voltage, and the heat accumulation in the resistive SFCL may cause a long quench recovery time. In [33,34], the scheme design and assessment of a modified flux-coupling-type SFCL for medium-scale wind plants with multiple DFIGs are studied, and the results imply that reducing the operation loss and cumulative heat of the SFCL is of significance. From this perspective, using an inductive current-limiting device is an alternate solution [35].

It is worthy to state that, a few preliminary studies on the coordination control of a fault current limiter and an energy storage device for stabilizing a DFIG have been reported [36–40]. It is revealed that the combined utilization of two devices with different functions can bring more contributions in enhancing the transient characteristics of a DFIG. In a sense, developing this kind of study and exploring a novel combination scheme with preferable potentials are of significance.

1.2 Contributions of this paper

In this paper, our research group proposes the coordination control of a DVR and an inductive FCL to improve a DFIG's LVRT capability. The DVR is located to the DFIG's stator circuit for stabilizing the terminal voltage and decreasing the generator current. The FCL is connected to the DFIG's rotor circuit for suppressing the rotor overcurrent and protecting the converter.

For the DFIG, employing the DVR is to offer a direct voltage compensation and an indirect current limitation. As the DVR is not good at decreasing the rotor current, a considerable DVR rating should be designed to make all LVRT criteria including the stator voltage, rotor current and electromagnetic torque be satisfied under the severe fault. When the inductive FCL cooperates with the DVR to handle the LVRT issue together, the direct contribution of the FCL in lowering the rotor current can effectively remedy the performance limitation of the DVR. Thus, the application of the FCL will bring a proper reduction in the DVR rating, and meanwhile the DVR alleviates the current-limiting pressure of the FCL.

The main contributions and novelty of this paper are summarized as follows:

1. Applying a DVR and an inductive FCL into different locations of a DFIG for its LVRT capability improvement.
2. Clarifying the theoretical effects of the combined DVR-FCL on the DFIG's transient behaviors.
3. Evaluating the effectiveness of the proposed approach in a typical DFIG under symmetrical and asymmetrical faults.

4. Performing a detailed comparative study of the proposed approach and the single action of DVR or FCL, in terms of the DFIG's voltage-current fluctuations, power delivery stability and electromagnetic torque oscillations.

1.3 Organization of this paper

The arrangement of this paper is as follows. Section 2 conducts the theoretical presentation of a DFIG. In Sections 3–4, the structural principle and coordinated method of a DVR and an inductive FCL for a DFIG are elaborated. In Section 5, simulation evaluation and performance comparison are implemented. Section 6 summarizes the main findings and explores the improvements in the future.

2 Theoretical Presentation of a typical DFIG based WT

Fig 1 shows the schematic of a typical DFIG based WT, which is accessed to the main network through a power transformer. By referring to [41], the modeling equations are formulated as:

$$\overrightarrow{V_s} = R_s \vec{i}_s + d\overrightarrow{\psi_s}/dt + \mathrm{j}\omega_s \overrightarrow{\psi_s} \tag{1}$$

$$\overrightarrow{V_r} = R_r \vec{i}_r + d\overrightarrow{\psi_r}/dt + \mathrm{j}(\omega_s - \omega_r)\overrightarrow{\psi_r} \tag{2}$$

$$\overrightarrow{\psi_s} = L_s \vec{i}_s + L_m \vec{i}_r \tag{3}$$

$$\overrightarrow{\psi_r} = L_m \vec{i}_s + L_r \vec{i}_r \tag{4}$$

where $\vec{i}, \overrightarrow{V}, \overrightarrow{\psi}, R, L$ are the current, voltage, flux, resistance as well as inductance, respectively. Subscripts s, r are the stator and rotor, respectively. It is obtained that $L_s = L_{s\sigma} + L_m$ and $L_r = L_{r\sigma} + L_m$, and $L_{s\sigma}/L_{r\sigma}$ is the leakage inductance.

In light of the Eqs (3) and (4), the stator and rotor currents are signified as:

$$\vec{i}_s = \overrightarrow{\psi_s}/L'_s - k_r \overrightarrow{\psi_r}/L'_s \tag{5}$$

$$\vec{i}_r = -k_s \overrightarrow{\psi_s}/L'_r + \overrightarrow{\psi_r}/L'_r \tag{6}$$

where $L'_s = L_s - L^2{}_m/L_r$ and $L'_r = L_r - L^2{}_m/L_s$ are deduced; k_s and k_r are expressed as $k_s = L_m / L_s$ and $k_r = L_m / L_r$, respectively.

Fig 2 shows the control block diagram of the DFIG converters. For the DFIG, the RSC is to adjust the rotor current and reactive power, and the GSC is to regulate the DC-link voltage and grid-side current [42,43]. A brief description of the adopted control strategy is as follows: (1) The rotor angular frequency ω_r is measured from the wind conditions, and the reference ω_{ref} is concerning maximum power point tracking. In light of the deviation $\Delta\omega$, the rotor current reference $i_{qr\text{-}ref}$ can be gained, and then a classical proportional-integral controller is used for the rotor current regulation. (2) The reference $V_{dc,ref}$ is regarding the DC-link nominal voltage, and a comparing control loop is constructed for the DC-link voltage maintenance. (3) The reactive power adjustments are implemented by both the RSC with the reference Q_{sref} and the GSC with the reference $Q_{gc,ref}$ [44]. Since this study focuses on exploring a hardware solution based on the combined DVR-FCL for the DFIG, our research group does not conduct additional modifications on the theory and control strategy of the DFIG controllers.

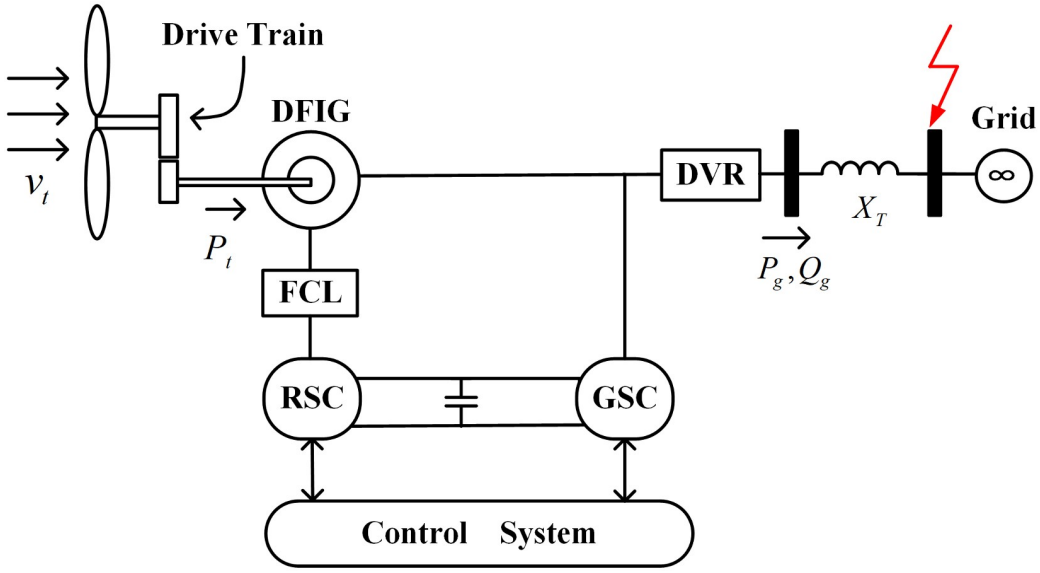

Fig 1. Schematic of a DFIG based WT with a DVR and an inductive FCL.

https://doi.org/10.1371/journal.pone.0221410.g001

3 Configuration of the DVR and its effects on the DFIG

Fig 3a denotes the schematic of a DVR, and Fig 3b gives the control block diagram [45,46]. From the suggested control, the DVR may inject a highly flexible and adjustable voltage in series with the generator terminal.

In this study, a voltage-drop coefficient A_1 ($0 \leq A_1 \leq 1$) is introduced for the DFIG, and the terminal voltage is expressed as:

$$\vec{V}_s = \begin{cases} V_s e^{j\omega_s t} & t < t_0 \\ (1 - A_1) V_s e^{j\omega_s t} & t \geq t_0 \end{cases} \tag{7}$$

where t_0 is the fault occurrence time.

Considering the voltage compensation by the DVR, its function is represented by a voltage-increase coefficient A_{DVR} ($0 \leq A_{DVR} \leq A_1$). Thereupon, the DFIG's terminal voltage will be rewritten as:

$$\vec{V}_s = \begin{cases} V_s e^{j\omega_s t} & t < t_0 \\ (1 - A_1 + A_{DVR}) V_s e^{j\omega_s t} & t \geq t_0 \end{cases} \tag{8}$$

By referring to the constant-linkage theory [47], the stator flux is:

$$\vec{\psi}_s = \begin{cases} \dfrac{L_s V_s}{R_s + j\omega_s L_s} e^{j\omega_s t} + \dfrac{R_s L_s I_r}{R_s + j\omega_s L_s} e^{j\omega_s t} & t < t_0 \\ \dfrac{L_s (1 - A_1 + A_{DVR}) V_s}{R_s + j\omega_s L_s} e^{j\omega_s t} + \dfrac{R_s L_s I_r}{R_s + j\omega_s L_s} e^{j\omega_s t} + \vec{\psi}_{s0} e^{-R_s t / L_s} & t \geq t_0 \end{cases} \tag{9}$$

where $\vec{\psi}_{s0}$ is to describe the natural component of the stator flux, and its expression is:

$$\vec{\psi}_{s0} = \frac{L_s (A_1 - A_{DVR}) V_s e^{j\omega_s t_0}}{R_s + j\omega_s L_s} \tag{10}$$

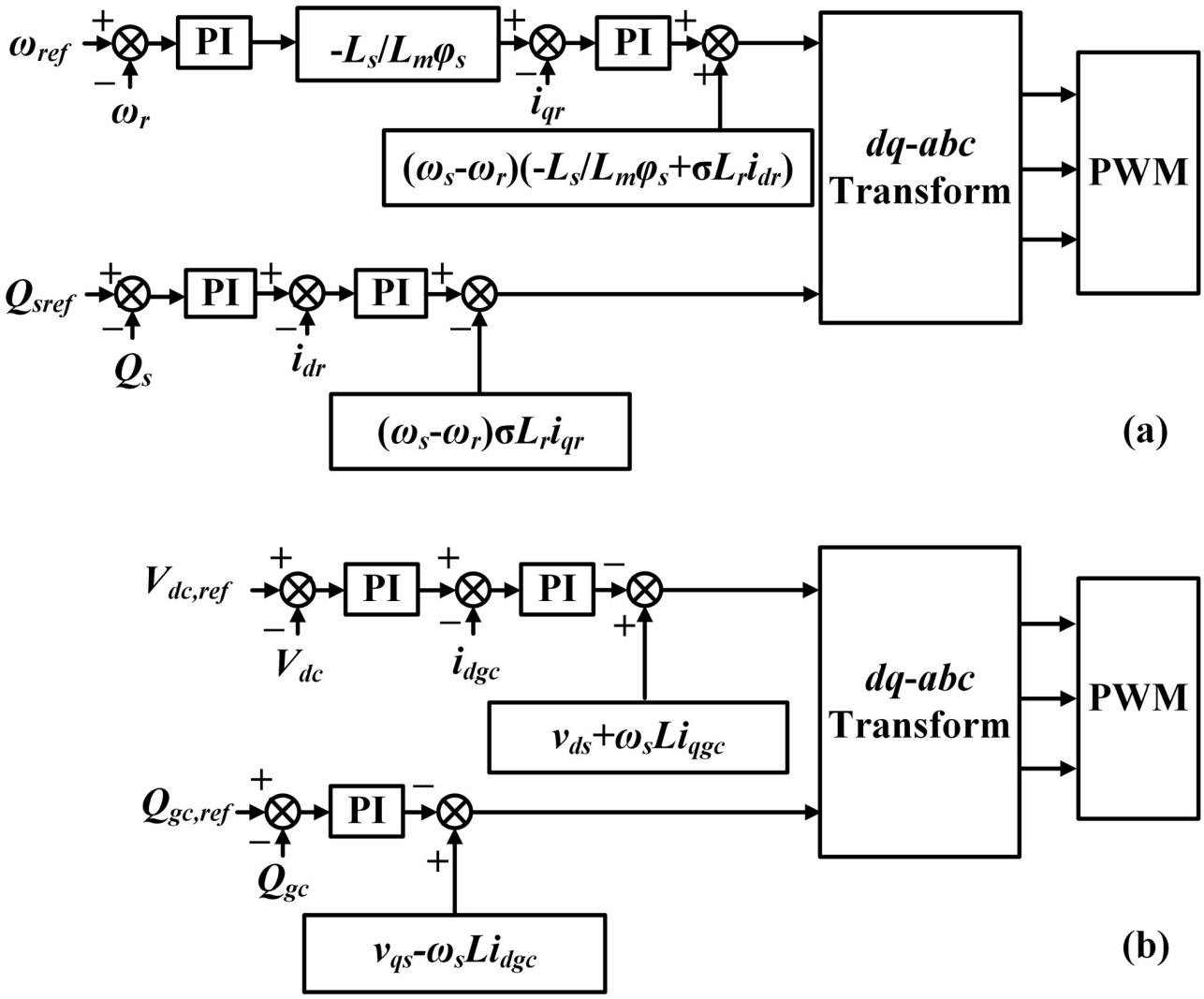

Fig 2. Control block diagram of the DFIG converters. (a) RSC, (b) GSC.

https://doi.org/10.1371/journal.pone.0221410.g002

By ignoring R_s in the Eq (9), the stator flux can be rewritten as:

$$\vec{\psi}_s = \begin{cases} \dfrac{V_s}{j\omega_s} e^{j\omega_s t} & t < t_0 \\ \dfrac{(1 - A_1 + A_{DVR})V_s}{j\omega_s} e^{j\omega_s t} + \dfrac{(A_1 - A_{DVR})V_s e^{j\omega_s t_0}}{j\omega_s} e^{-\frac{R_s}{L_s}t} & t \geq t_0 \end{cases} \tag{11}$$

Thus, in combination with the Eq (3), the stator current will be deduced as:

$$\vec{i}_s = \frac{(A_1 - A_{DVR})V_s e^{j\omega_s t_0}}{j\omega_s L_s} e^{-\frac{R_s}{L_s}t} + \frac{(1 - A_1 + A_{DVR})V_s}{j\omega_s L_s} e^{j\omega_s t} - \frac{L_m \vec{i}_r}{L_s} \tag{12}$$

From the above theoretical derivations, introducing the DVR is able to offer a direct effect on alleviating the stator-voltage drop, and meanwhile, the fault current in the stator side can be potentially suppressed.

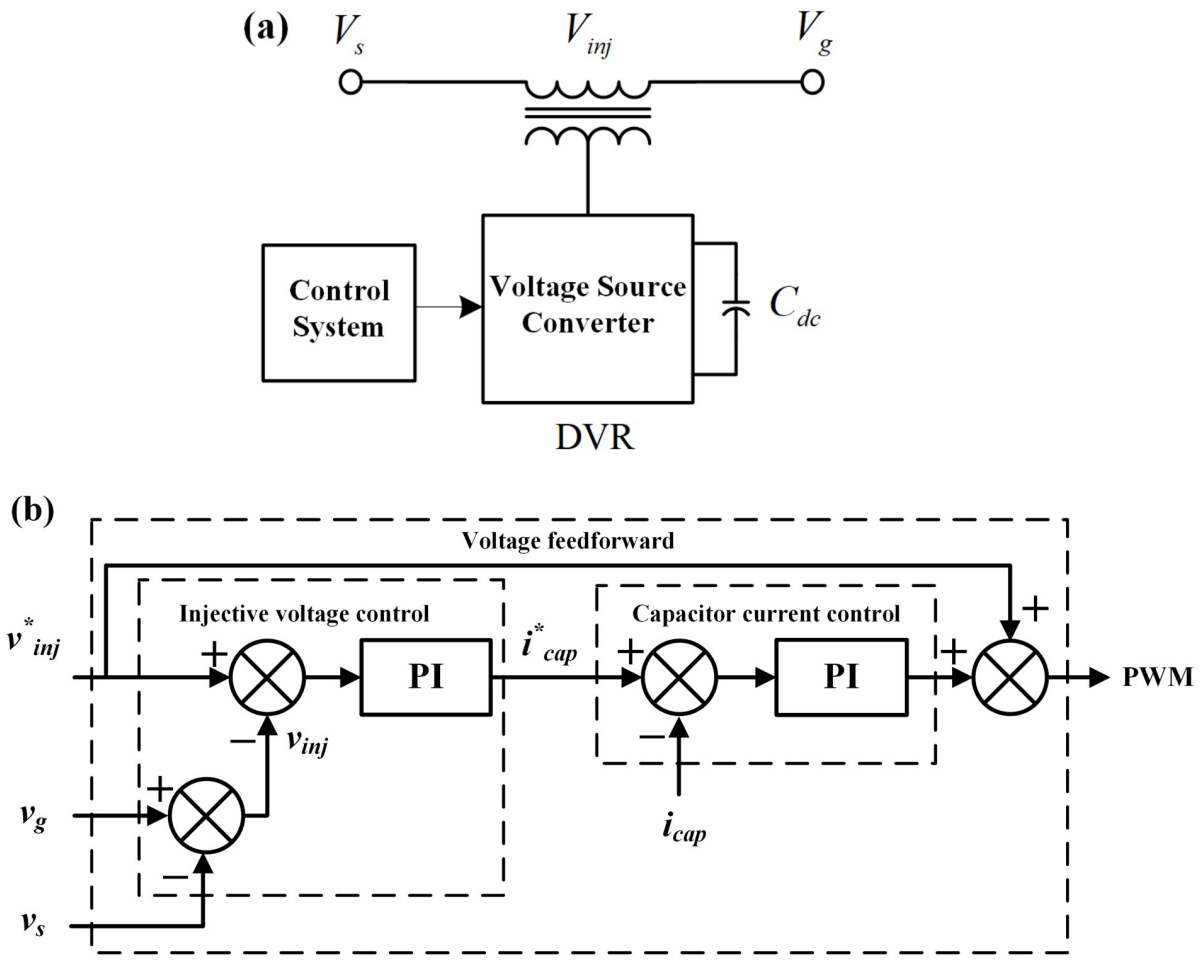

Fig 3. Description of the DVR. (a) Schematic, (b) control block diagram.

https://doi.org/10.1371/journal.pone.0221410.g003

4 Structure, control and influence of the inductive FCL for the DFIG

After the expected effects of the DVR are exploited, the inductive FCL should be quickly triggered. Fig 4 shows the topological structure of the inductive FCL, and by controlling the status of the switch S_{cs}, the current-limiting inductance of $Z_{FCL} \approx j\omega L_{ct2}$ can be activated in time [48,49].

Fig 5 shows the equivalent circuit of the RSC with the inductive FCL. Herein, R_{3r} and C_{3r} represent the filtering resistance and capacitance, respectively. This resistance-capacitance branch can join the leakage inductance of the FCL and the rotor to form a LCL filter with the low-pass feature. Then, the rotor voltage mainly appears the frequency component, and according to the rotor back-electromagnetic force (EMF) [50], the voltage equation is derived as:

$$\vec{V_r} = R_r \vec{i_r} + (\sigma L_r + L_{FCL}) \frac{d}{dt} \vec{i_r} + \vec{e_r} \tag{13}$$

where σL_r is denoted as the rotor transient inductance; $\vec{e_r}$ is the EMF induced at the rotor

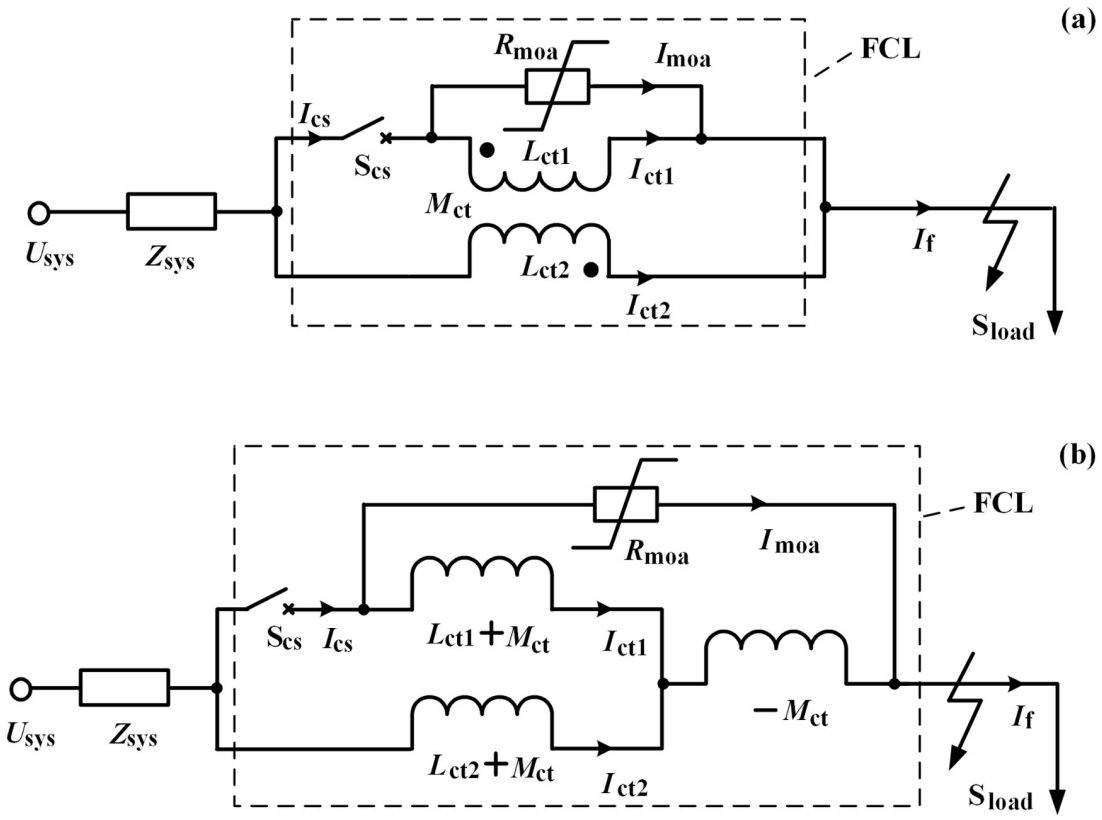

Fig 4. Topological structure of the inductive FCL. (a) Main connection, (b) equivalent circuit.

https://doi.org/10.1371/journal.pone.0221410.g004

side, and its expression is:

$$\overrightarrow{e_r} = \begin{cases} k_s V_s e^{j\omega_s t} & t < t_0 \\ k_s s(1 - A_1 + A_{DVR}) V_s e^{j\omega_s t} - (1 - s) k_s (A_1 - A_{DVR}) V_s e^{-j(1-s)\omega_s t} e^{-\frac{R_s}{L_s} t} & t \geq t_0 \end{cases} \quad (14)$$

where s is used to denote the slip with the range of [-0.3, 0.3].

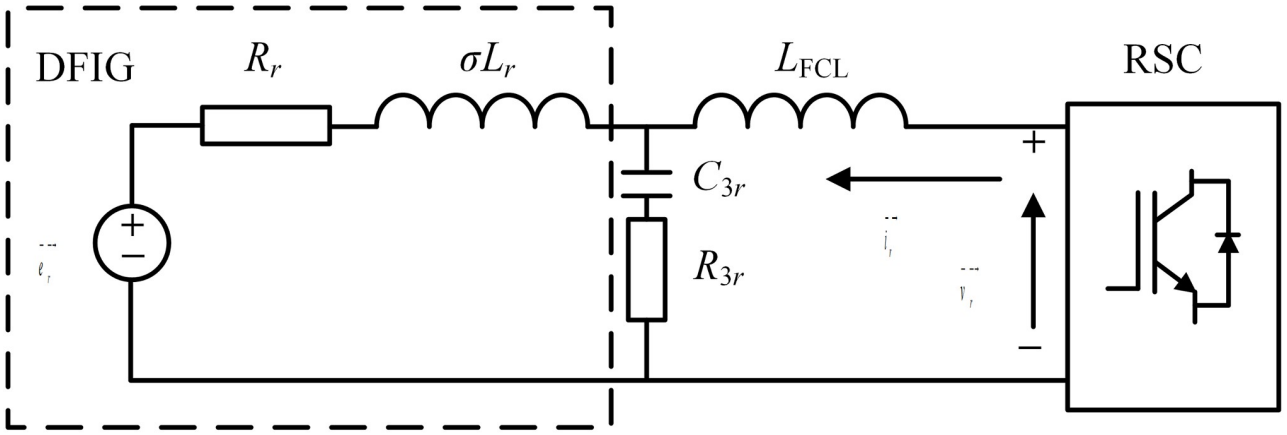

Fig 5. Equivalent circuit analysis of the RSC with the FCL.

https://doi.org/10.1371/journal.pone.0221410.g005

Table 1. Main parameters of the DFIG with the combined DVR-FCL.

FCL	Primary/Secondary/Mutual inductance	6 mH/6 mH/5.99 mH
	Coupling Coefficient k	0.999
DVR	Rated capacity	0.75 MW
	Filtering capacitance	0.1 mH
	Filtering inductance	1 μF
	Switching frequency	10 kHz
	Series transformer ratio	1
DFIG based WT	Rated capacity	1.5 MW
	Rated wind speed	11 m/s
	Stator voltage / frequency	690 V / 50 Hz
	Rotor voltage / frequency	2370 V / 12 Hz
	Stator resistance / leakage inductance	0.023 pu / 0.18 pu
	Rotor resistance / leakage inductance	0.016 pu / 0.16 pu
	DC-link voltage	1150 V

https://doi.org/10.1371/journal.pone.0221410.t001

During the transient process, the rotor current could be contributed by three components [51]. The first component is feed by the voltage applied to the rotor circuit; the second component is feed by the forced component of the rotor open voltage; the third component is a dc component damping in an exponential way. Thus, considering the impacts of the combined DVR-FCL, the rotor current is expressed as:

$$\begin{aligned}\vec{i}_r = &\frac{V_{rc} - k_s s(1 - A_1 + A_{DVR})V_s}{R_r + \mathrm{j}s\omega_s(\sigma L_r + L_{FCL})} e^{\mathrm{j}s\omega_s t} + \frac{k_s(1-s)(A_1 - A_{DVR})V_s}{R_r - \mathrm{j}(1-s)\omega_s(\sigma L_r + L_{FCL})} e^{-\mathrm{j}(1-s)\omega_s t} e^{-\frac{R_s}{L_s}t} \\ &+ \left[\frac{V_r - V_{rc} - k_s s(A_1 - A_{DVR})V_s}{R_r + \mathrm{j}s\omega_s(\sigma L_r + L_{FCL})} - \frac{k_s(1-s)(A_1 - A_{DVR})V_s}{R_r - \mathrm{j}(1-s)\omega_s(\sigma L_r + L_{FCL})}\right] e^{-\frac{R_r}{L_r + L_{FCL}}t}\end{aligned} \tag{15}$$

where V_{rc} denotes the rotor open voltage.

From the Eq (15), adjusting the parameters of the DVR (A_{DVR}) and the FCL (L_{FCL}) will both affect the rotor current limitation. Herein, a simplified calculation of the rotor current is done, and it is assumed that $A_1 = 1$, $k_s \approx 1$, $A_{DVR} = 0$ and $R_r \approx 0$. Thereupon, the maximum rotor current is approximatively written as:

$$|\vec{i}_r|_{\max} \leq \frac{V_r + sV_s}{s\omega_s(\sigma L_r + L_{FCL})} \tag{16}$$

According to the Eq (16), the relation between the maximum rotor current and the inductance L_{FCL} can be roughly determined, and after the DVR is applied, the parameter setting of L_{FCL} will be properly decreased.

5 Simulation analysis

To validate the effectiveness and feasibility of the proposed approach, simulation analyses are done in MATLAB, and Table 1 summarizes the parameters. Regarding the design criteria for DVR and FCL, an explanation is given. For only using a DVR in a DFIG, the DVR capacity can be equal to the rated power of the DFIG, and this original design criterion is adopted in [21]. Since the application of the FCL can alleviate the DVR rating, this study doesn't use the original design criteria. Correspondingly, it is designed that the DVR capacity is half of the DFIG power rating, and the FCL rating is based on a reasonable reduction in the flux-coupling-type FCL rating [27]. As the inductive FCL has a relatively simple structure, the

economic performance of the inductive FCL is generally superior to that of the DVR [52], and it means that the proposed scheme (a half compensation DVR and an inductive FCL) may offer better economic performance than a full compensation DVR. Note that, the parameters of the FCL and DVR have not been fully optimized. Aiming at their different costs and contributions to the DFIG's LVRT operation, a detailed capacity optimization study will be presented in another report.

5.1 Study of the symmetrical fault

It is simulated that a three-phase fault occurs at $t = 1$ s, and the fault duration is 200 ms. Fig 6 shows the DFIG terminal voltage in the event of without auxiliary. Herein, the range of time-axis is set as [0.94 s, 1.06 s], and it is expected to more clearly show the voltage change before and after the fault. Both the instantaneous value and Root-Mean-Square (RMS) value are given, and when the steady peak value of the terminal voltage (standard sinusoidal wave) is 1.0 pu, the RMS value is calculated as $\frac{1}{\sqrt{2}} = 0.707$pu. Under the fault, the generator voltage declines sharply, and the caused transient phenomena are very strong. During the simulations, we consider four different cases, which are expressed as without auxiliary, only with the DVR, only with the FCL, and with the DVR-FCL. The criteria regarding the LVRT behaviors are described as that: (1) The generator voltage satisfies the Denmark code. The DFIG needs to hold its connection state at least for 150 ms when the terminal voltage drops to 20% of the nominal level. Meanwhile, the generator voltage should recovery to 75% of nominal level within about 0.7 s. (2) The limit of the rotor current is set as 2.0 pu [53,54]. (3) The DC-link voltage is lower than 1.35 kV. (4) The electromagnetic torque is not exceeding 2 ~ 2.5 pu [55–57].

Figs 7 and 8 show the DFIG stator and rotor current characteristics. Obviously, the combined DVR-FCL performs the best functions in suppressing the fault currents, and an adequate safety margin will be caused for supporting the LVRT operation. It should be pointed out that, only with the DVR is insufficient to make the DFIG ride through the fault, as the rotor current is still larger than the allowable limit.

Fig 9 denotes the RMS feature of the DFIG terminal voltage, where the phase-A is selected. The symmetrical fault causes a very serious voltage decline, and using the DVR can compensate the voltage to 50% of the nominal level. Whereas, the FCL has almost no influence on the terminal voltage. The simulation results show that the terminal voltage will start recovery at 1.2 s, where the short-circuit fault is exactly removed. According to the Denmark code, it implies that, if the wind generator expects to ride through a short-circuit fault with a little longer duration (200 ms), a higher terminal voltage level during the fault should be reached (25% of the nominal level). From this perspective, considering the favorable voltage compensation by the DVR-FCL, the DFIG can be soundly connected to the main network for 0.46 s, which is greatly more than the fault duration. Therefore, an adequate time margin is obtained for keeping the connection state of the DFIG.

In practice, when the DFIG fails to meet the LVRT criteria, it will be disconnected, and the terminal voltage cannot be recovered timely until the reconnection is done. To observe the possible dynamic fluctuations, we do not simulate the action of shutting down the wind generator even if it has an insufficient LVRT capability. Thus, for without auxiliary, the DFIG terminal voltage can favorably recover to the normal condition after the fault is removed. Also, the combined DVR-FCL has a moderate ability to accelerate the voltage recovery.

Figs 10–12 show the DFIG active power, electromagnetic torque and DC-link voltage during the fault, and the performance data of the selected four cases are indicated in Table 2. From the results, the combined DVR-FCL provides the best contributions in stabilizing the

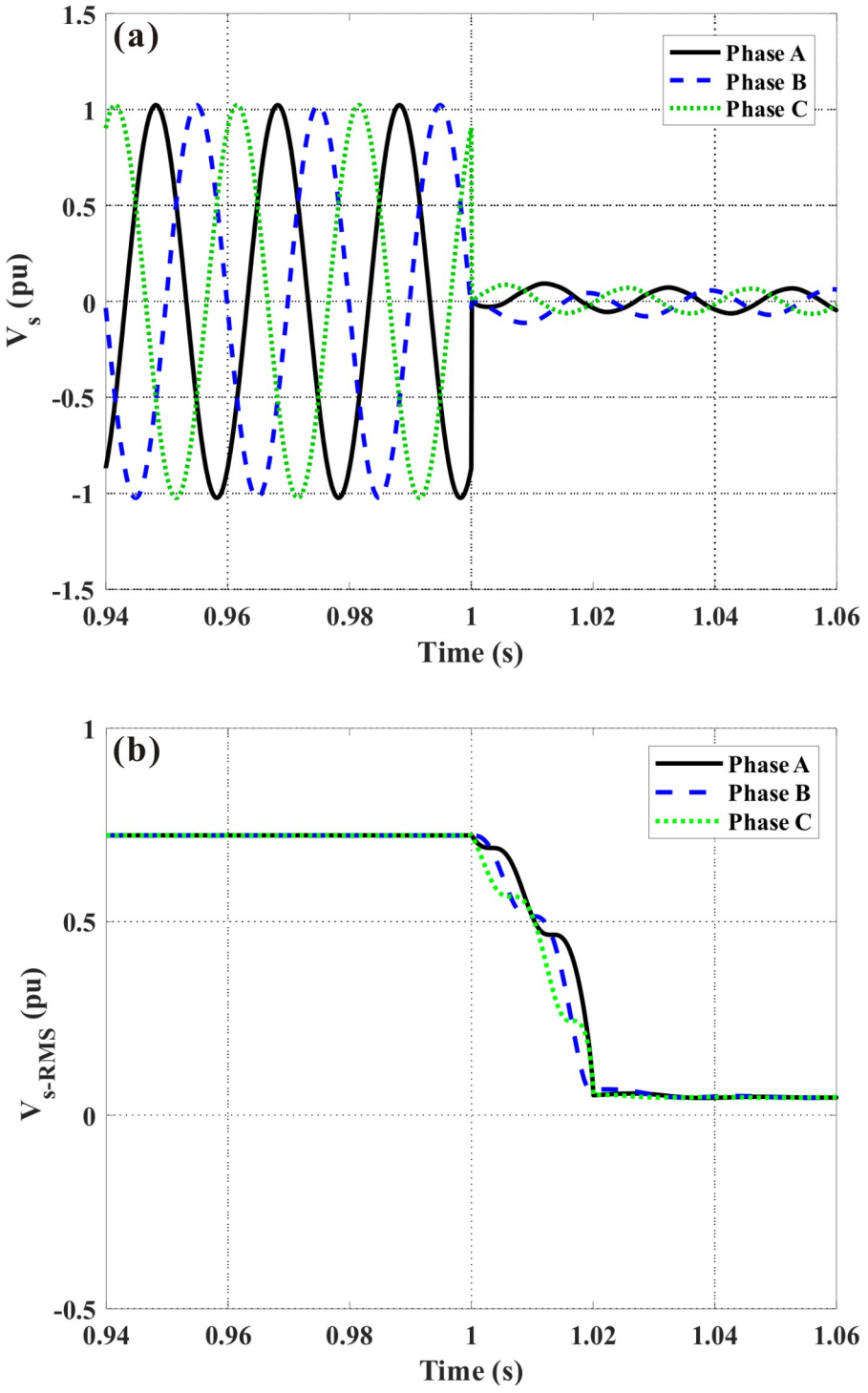

Fig 6. DFIG terminal voltage subject to the symmetrical fault. (a) Instantaneous value, (b) RMS value.

https://doi.org/10.1371/journal.pone.0221410.g006

DFIG. The generator power is controlled at ~1 MW, and the electromagnetic torque is inhibited at 0.97 pu.

Based on the simulations of the DC-link overvoltage, a technical discussion is as follows. The DC-link voltage is mainly determined by its excess power and the GSC's adjusting ability.

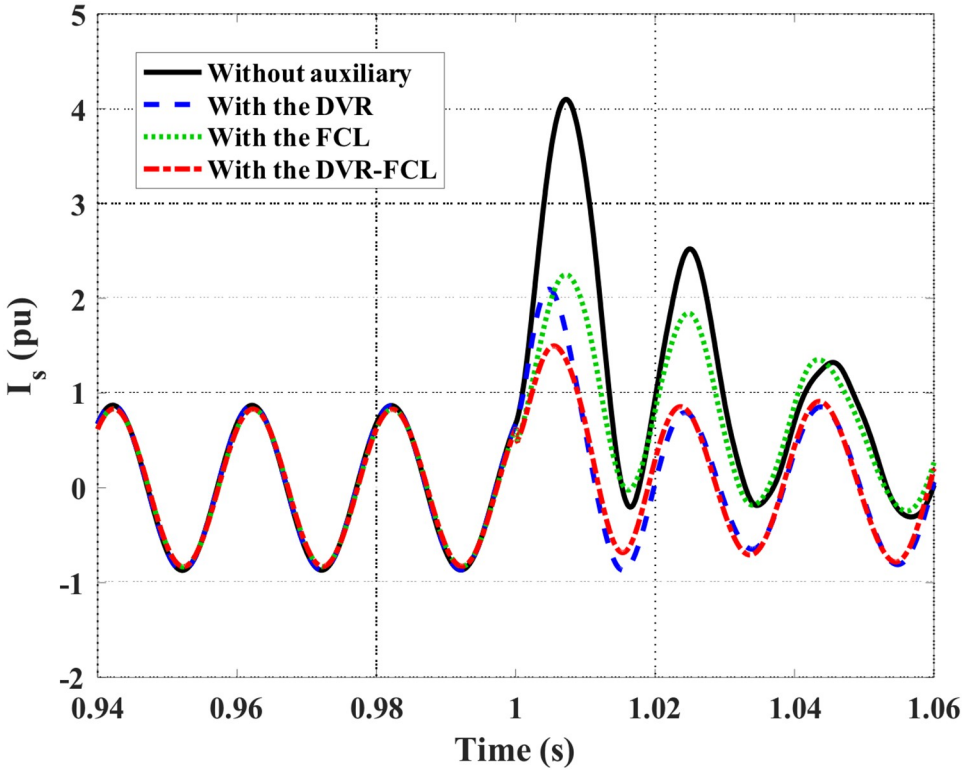

Fig 7. Stator current of the DFIG subject to the symmetrical fault.

https://doi.org/10.1371/journal.pone.0221410.g007

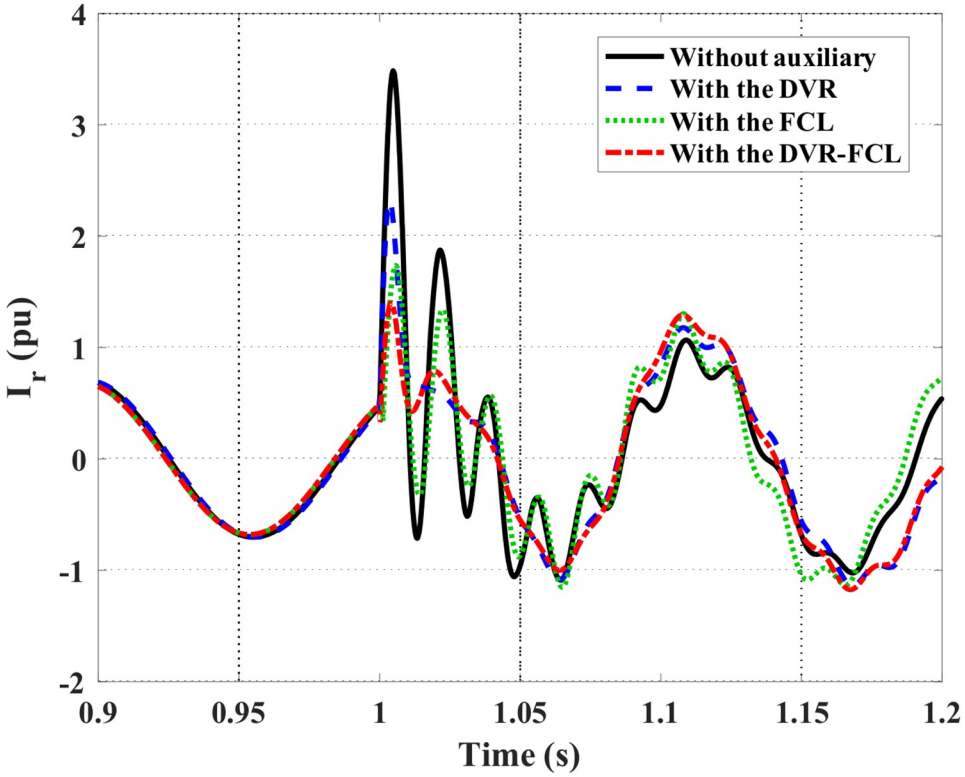

Fig 8. Rotor current of the DFIG subject to the symmetrical fault.

https://doi.org/10.1371/journal.pone.0221410.g008

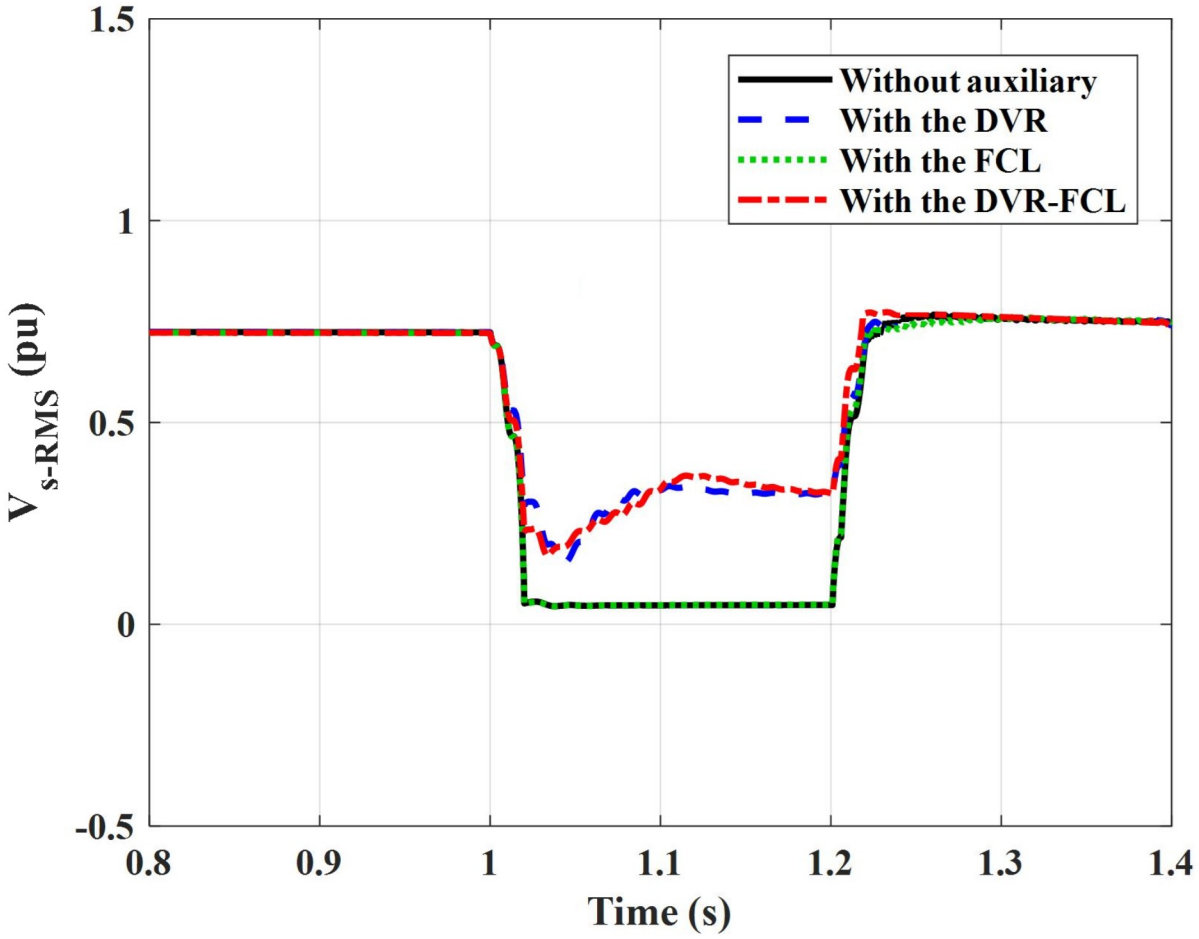

Fig 9. RMS value of the DFIG terminal voltage subject to the symmetrical fault.

https://doi.org/10.1371/journal.pone.0221410.g009

For without auxiliary, the larger stator current makes the GSC leave the linear control region, and the higher rotor current causes a considerable oscillation power. It is inevitable that the DC-link voltage fluctuates and increases sharply. For with the FCL, the constrained rotor current makes the oscillation power be lowered, and due to the coupling between the rotor and stator, the GSC's adjusting ability can be appropriately improved. As affected by these two contributions, the FCL reduces the overvoltage level, but keeps the voltage pattern as the case without auxiliary.

For that the DVR is adopted, the above two benefits can be mildly remained, and also an enhanced terminal voltage increases the power stability of the DFIG. The excess power at the DC-link is accordingly mitigated, and it is a significant difference from the case with the FCL. In consequence, the DVR well outperforms the FCL to stabilize the DC-link overvoltage. That is why the cases with the DVR and the combined DVR-FCL do not follow the same pattern as the case with the FCL.

5.2 Study of the asymmetrical fault

It is simulated that a double-phase (phase-A and phase-B) fault happens at $t = 1$ s, and the fault duration is 200 ms. For the reasons why the most common single-phase fault is not chosen,

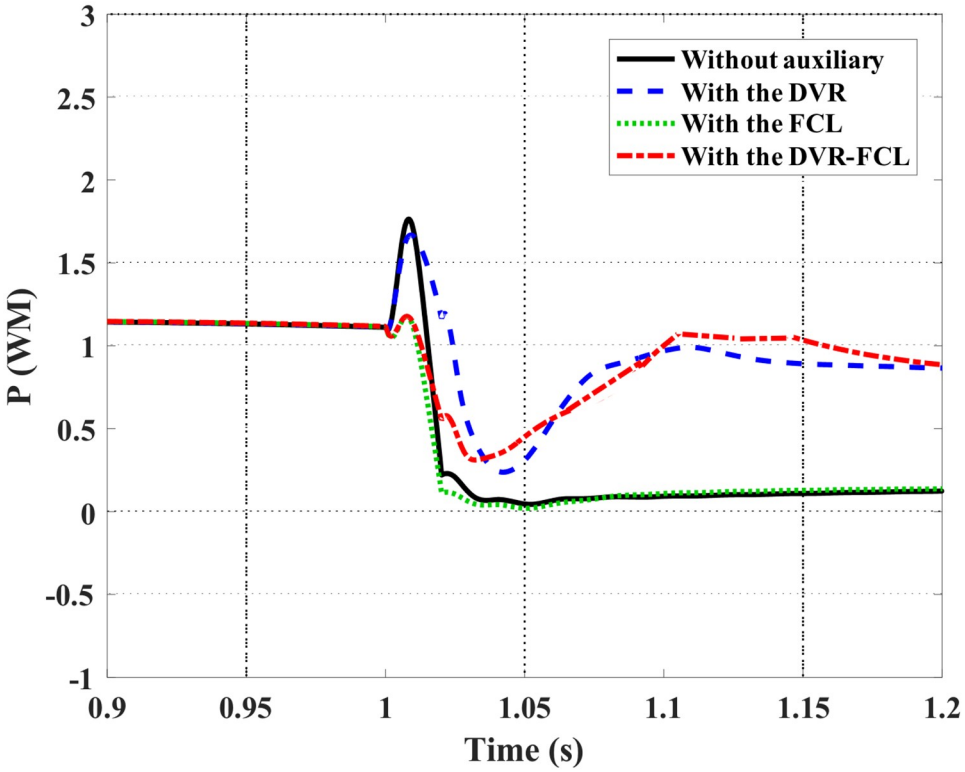

Fig 10. Active power of the DFIG subject to the symmetrical fault.

https://doi.org/10.1371/journal.pone.0221410.g010

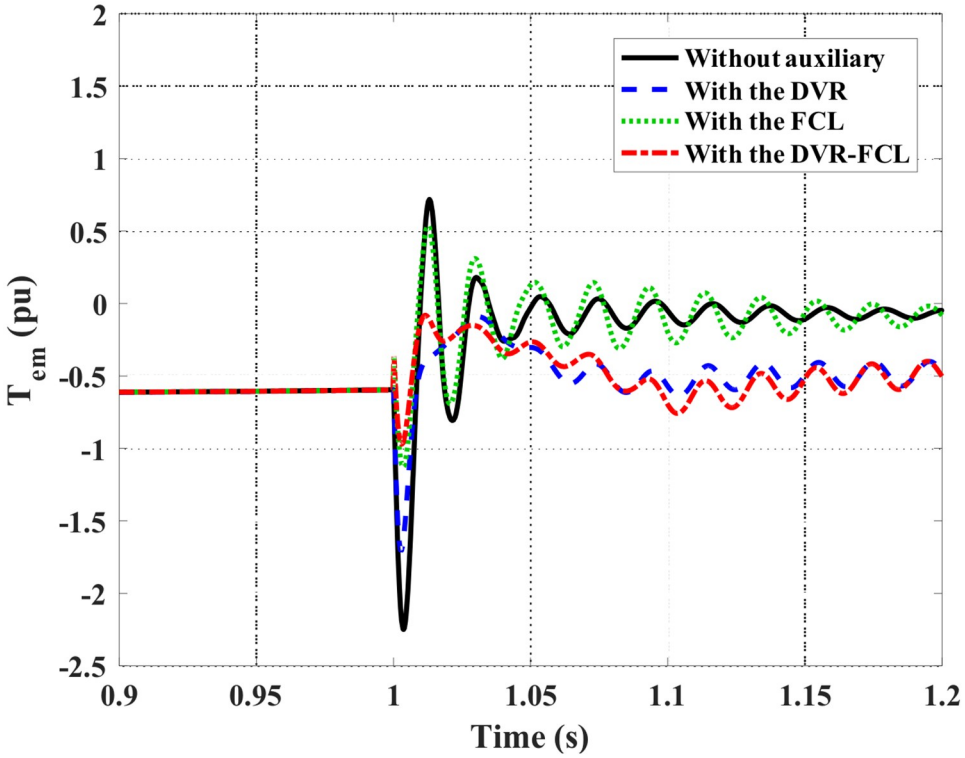

Fig 11. Electromagnetic torque of the DFIG subject to the symmetrical fault.

https://doi.org/10.1371/journal.pone.0221410.g011

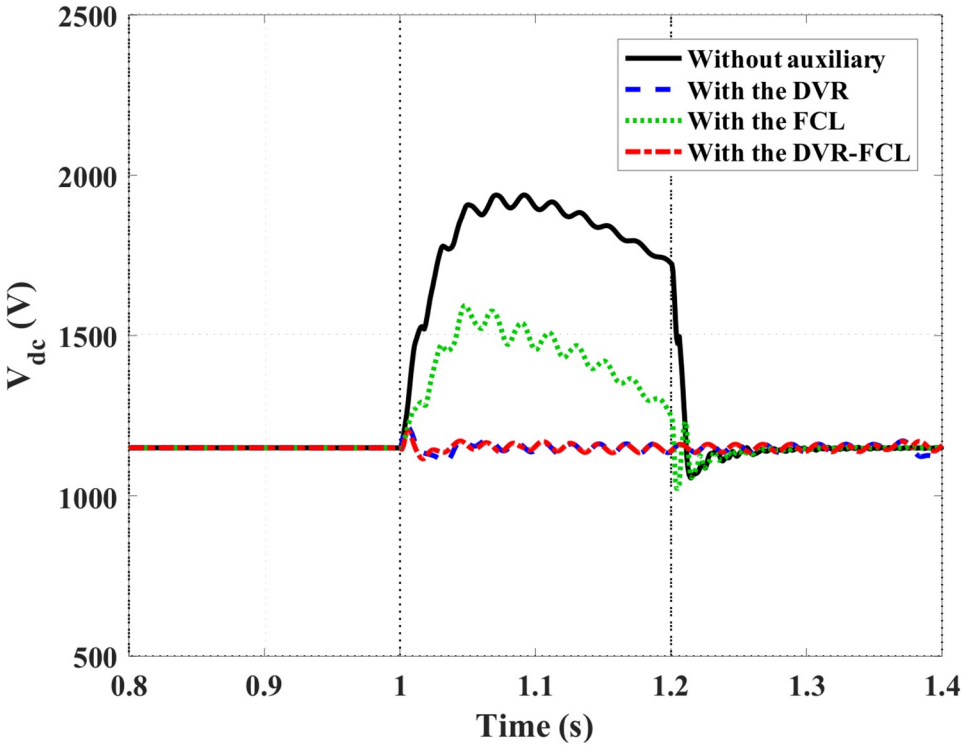

Fig 12. DC-link voltage of the DFIG subject to the symmetrical fault.

https://doi.org/10.1371/journal.pone.0221410.g012

our research group is to assess the effectiveness of the proposed approach to handle an asymmetrical fault with higher severity. If the combined DVR-FCL is capable of solving the double-phase fault problem, it is believed that the approach is also competent for handling the single-phase fault.

Fig 13 shows the DFIG terminal voltage during the asymmetrical fault. For without auxiliary, the RMS voltages of the two faulty phases (phase-A and phase-B) are decreased to 0.39 pu (55.2% of the nominal level) and 0.28 pu (39.6% of the nominal level), respectively. There is an ignorable voltage decline on the unfaulty phase, and the RMS voltage is kept at 94% of the nominal level. Fig 14 indicates the voltage compensation effects by various methods. It is clearly seen that the combined DVR-FCL brings the best voltage improvement. The DVR will firstly inject the voltage compensation on the two faulty phases, whose voltages are adjusted to be approximately equal with each other. Later, the inductive FCL will be activated to insert the desirable current-limiting inductance to the rotor circuit. From the results, the RMS voltages of the two faulty phases are enhanced to 0.56 pu (79.2% of the nominal level) and 0.61 pu

Table 2. Comparison of various methods on the DFIG subject to the symmetrical fault.

Items	Without auxiliary	With the DVR	With the FCL	With the DVR-FCL
Stator current	4.1 pu	2.1 pu	2.25 pu	1.49 pu
Rotor current	3.49 pu	2.31 pu	1.74 pu	1.4 pu
Terminal voltage (RMS)	0.05 pu	0.36 pu	0.06 pu	0.37 pu
Electromagnetic torque	2.25 pu	1.71 pu	1.13 pu	0.97 pu
DC-link voltage	1.94 kV	1.23 kV	1.59 kV	1.19 kV

https://doi.org/10.1371/journal.pone.0221410.t002

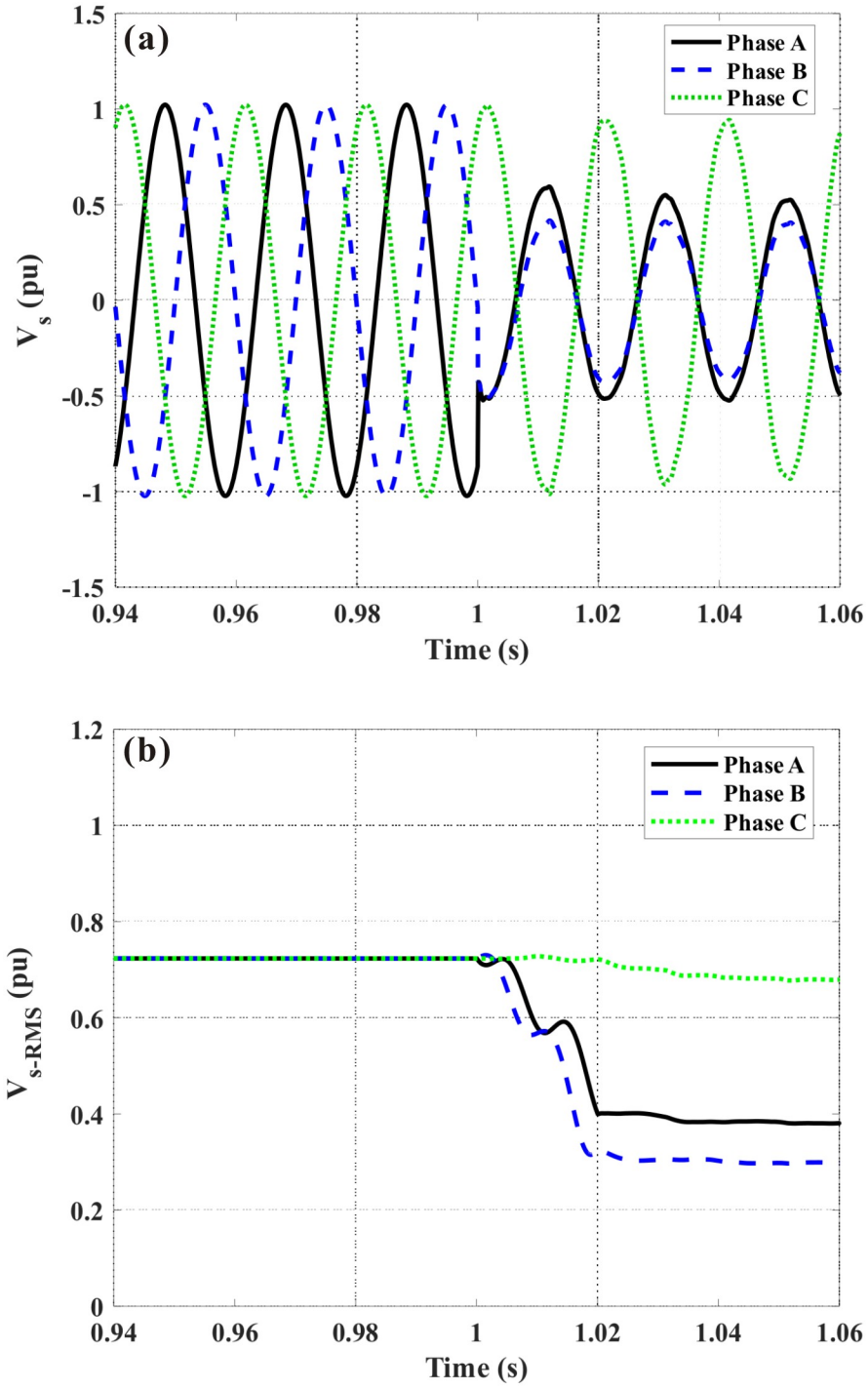

Fig 13. DFIG terminal voltage subject to the asymmetrical fault. (a) Instantaneous value, (b) RMS value.

https://doi.org/10.1371/journal.pone.0221410.g013

(86.3% of the nominal level) by using the combined DVR-FCL, and the voltage drop rates are about 20.8% and 13.7%, respectively.

Figs 15–19 show the DFIG stator and rotor currents, active power, electromagnetic torque and DC-link voltage subject to the asymmetrical fault. The detailed comparison of various

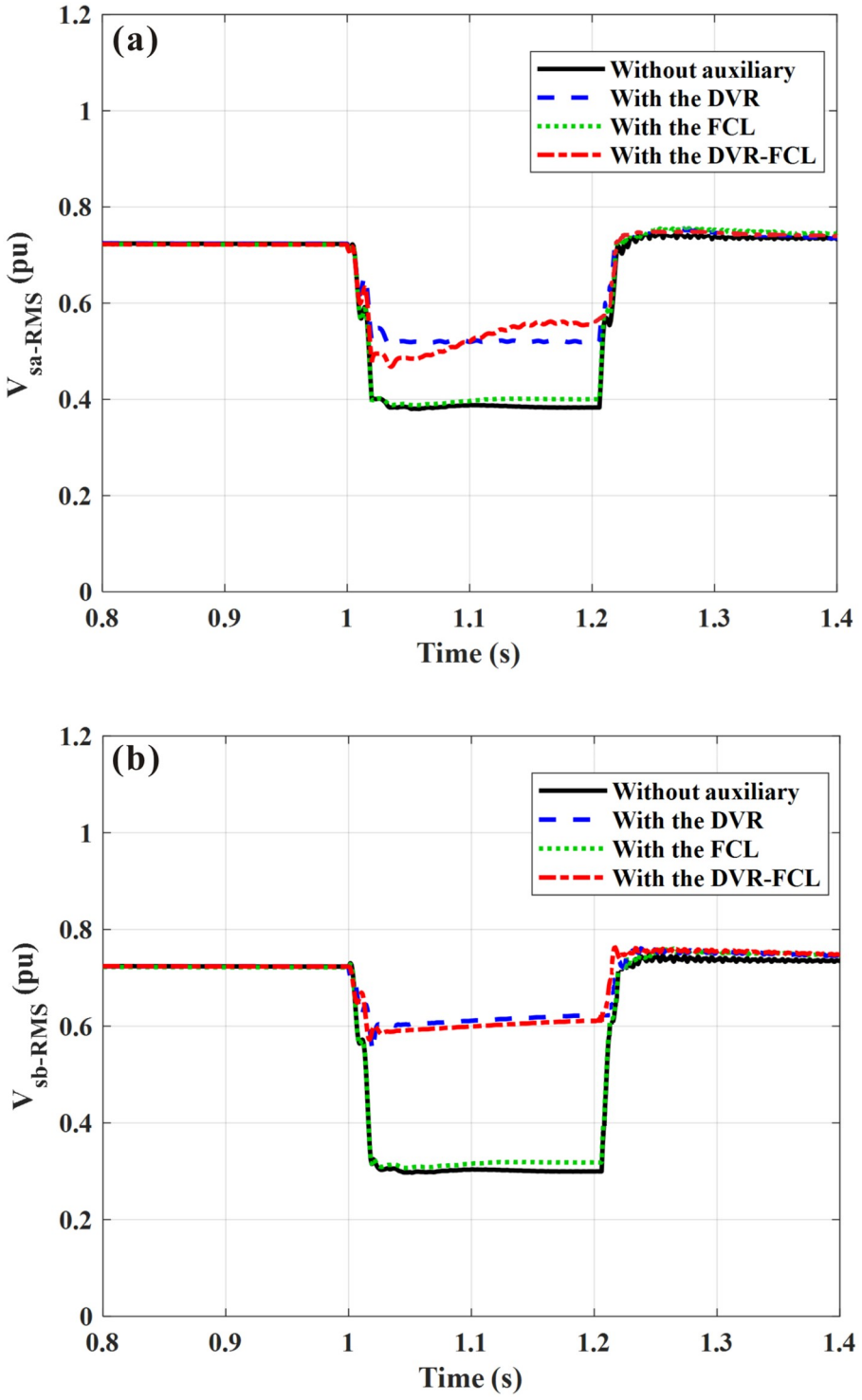

Fig 14. RMS value of the DFIG terminal voltage subject to the asymmetrical fault. (a) phase-A voltage, (b) phase-B voltage.

https://doi.org/10.1371/journal.pone.0221410.g014

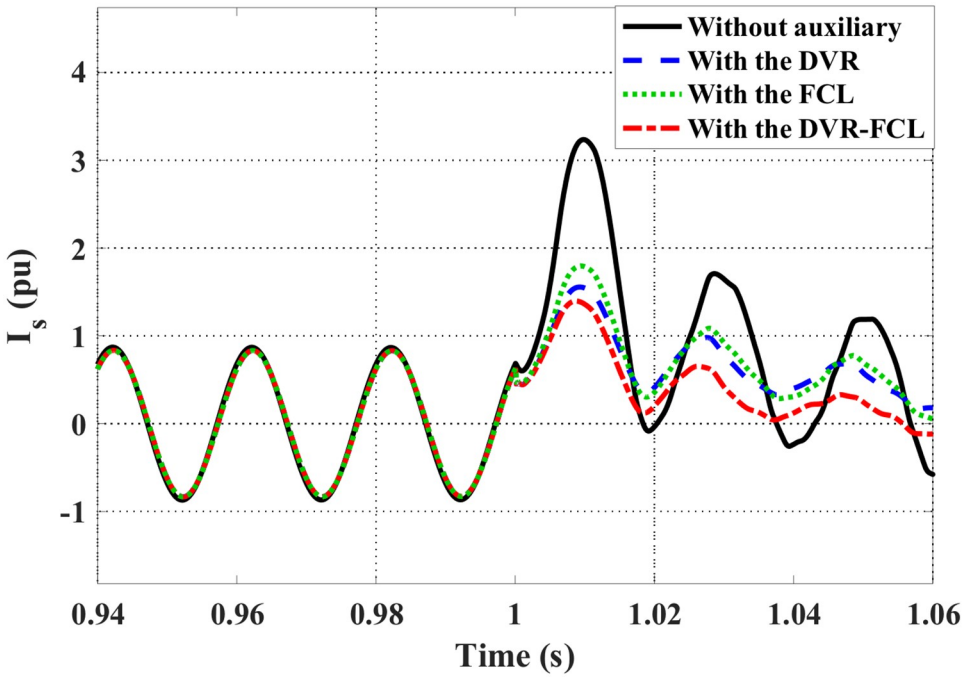

Fig 15. DFIG stator current subject to the asymmetrical fault.

https://doi.org/10.1371/journal.pone.0221410.g015

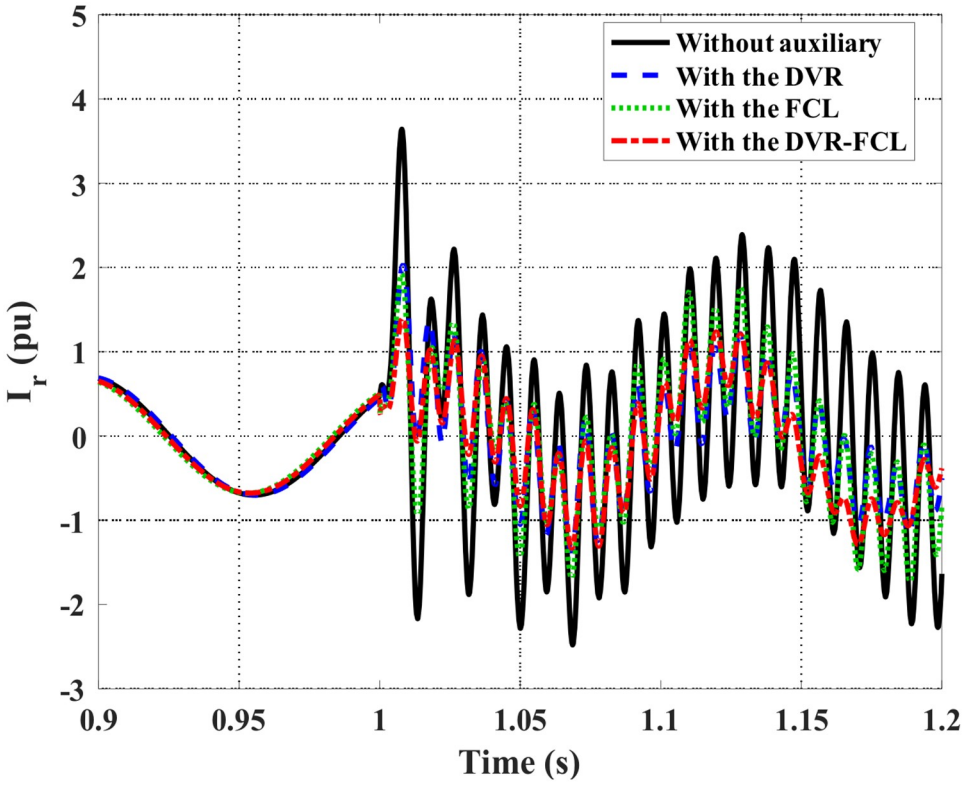

Fig 16. DFIG rotor current subject to the asymmetrical fault.

https://doi.org/10.1371/journal.pone.0221410.g016

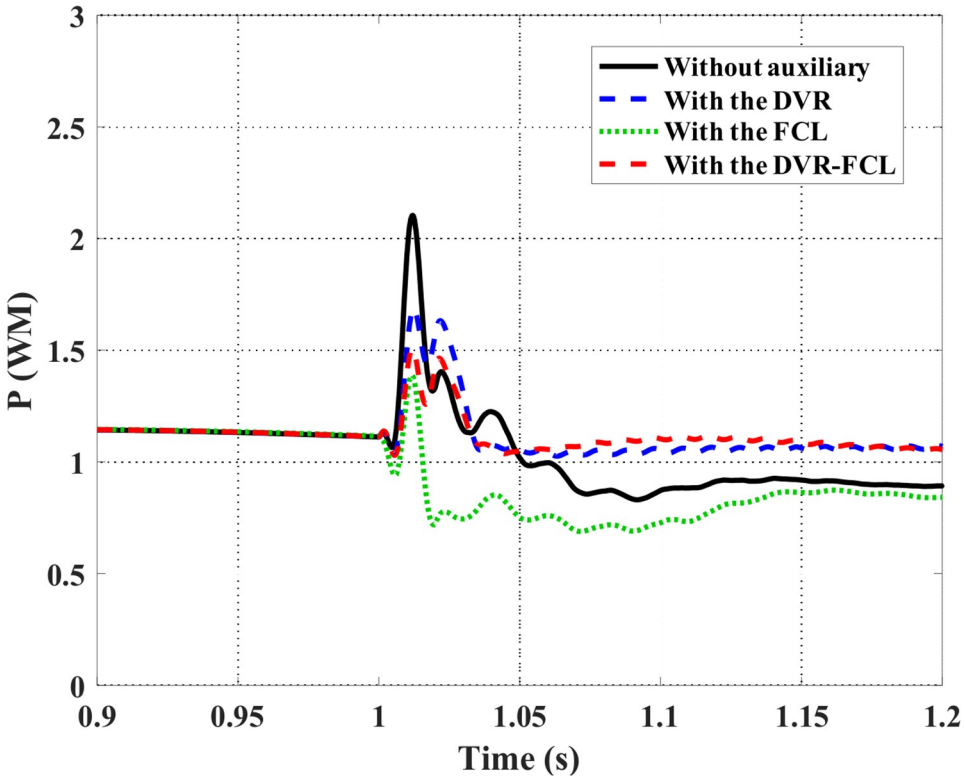

Fig 17. Active power of the DFIG subject to the asymmetrical fault.

https://doi.org/10.1371/journal.pone.0221410.g017

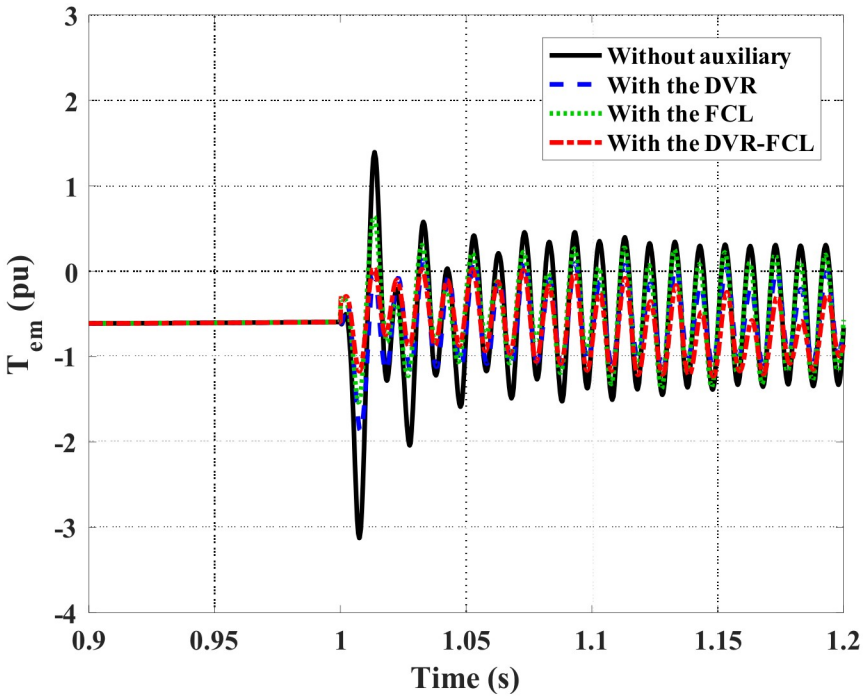

Fig 18. Electromagnetic torque of the DFIG subject to the asymmetrical fault.

https://doi.org/10.1371/journal.pone.0221410.g018

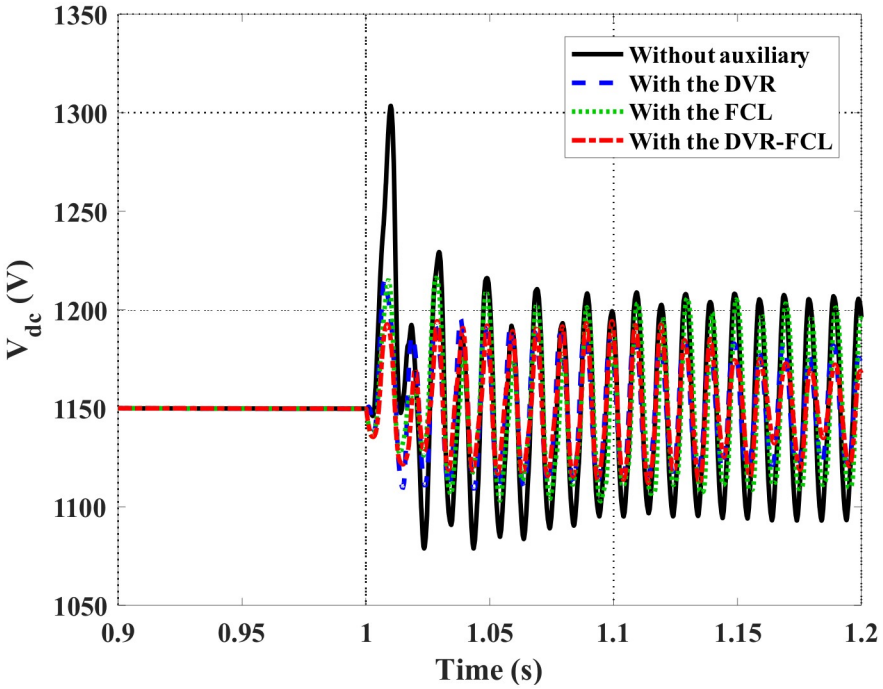

Fig 19. DC-link voltage of the DFIG subject to the asymmetrical fault.

https://doi.org/10.1371/journal.pone.0221410.g019

methods is listed in Table 3. Herein, the single action of the DVR or the FCL may not avoid disconnection of the DFIG, since the rotor current is exactly around its safety limit. After the combined DVR-FCL is utilized, the rotor current is suppressed to 1.35 pu, and the current-limiting ratio is up to 63%.

The maximum power fluctuation is ~1 MW when without auxiliary. For that the combined DVR-FCL is used, the GSC and RSC both operate in the linear regions, and multiple benefits are obtained for power stabilization of the DFIG. One is to limit the maximum fluctuation within the level of 0.4 MW, and the other is to keep the generator power at the level of 1.08 MW.

As compared to the symmetrical fault, it is clearly seen that the asymmetrical fault causes more obvious oscillations in the electromagnetic torque and the DC-link voltage. With regard to the contributions of the combined DVR-FCL, the maximum electromagnetic torque is reduced from 3.12 pu to 1.17 pu, and it is helpful to alleviate mechanical stress on the turbine. Furthermore, the DC-link voltage is limited to 1.19 kV, and the oscillation range is controlled within 60 V.

Table 3. Comparison of various methods on the DFIG subject to the asymmetrical fault.

Items	Without auxiliary	With the DVR	With the FCL	With the DVR-FCL
Stator current	3.28 pu	1.54 pu	1.81 pu	1.39 pu
Rotor current	3.64 pu	2.03 pu	1.92 pu	1.35 pu
Terminal voltage (RMS)	0.38 pu	0.54 pu	0.39 pu	0.56 pu
Electromagnetic torque	3.12 pu	1.88 pu	1.55 pu	1.17 pu
DC-link voltage	1.31 kV	1.21 kV	1.22 kV	1.19 kV

https://doi.org/10.1371/journal.pone.0221410.t003

6 Conclusions

This paper proposes an efficient LVRT scheme based on the coordination control of a DVR and an inductive FCL for a DFIG. Theoretical investigation and simulation analysis are done to validate the effectiveness of the proposed scheme. The combined DVR-FCL can powerfully decrease the fault currents in the DFIG stator and rotor, and perform visible voltage stabilization on the generator terminal and the DC-link. Additionally, the combined DVR-FCL enables to well strengthen the DFIG power stability and suppress the electromagnetic torque within the safety limit. In consequence, the risks to cause damage of the converters are avoided, and an adequate LVRT operation is realized for the DFIG under symmetrical and asymmetrical faults.

In the near future, the follow-on tasks for the proposed approach will be carried out, and they include parameter optimization, economic evaluation and prototyping test of the combined DVR-FCL in the DFIG. The specific research schemes and results will be addressed in other reports.

Author Contributions

Conceptualization: Dongyin Zhang, Lei Chen.

Data curation: Hanping Xu, Li Qiao.

Formal analysis: Li Qiao.

Funding acquisition: Lei Chen.

Investigation: Dongyin Zhang.

Methodology: Hanping Xu.

Software: Hanping Xu, Li Qiao.

Validation: Li Qiao, Lei Chen.

Writing – original draft: Dongyin Zhang.

Writing – review & editing: Lei Chen.

References

1. Liao S.; Yao W.; Han X.; Wen J.; Cheng S. Chronological operation simulation framework for regional power system under high penetration of renewable energy using meteorological data. *Appl. Energy* 2017, 203, 816–828.
2. Liu J.; Yao W.; Wen J.; Fang J.; Jiang L.; He H.; et al. Impact of power grid strength and PLL parameters on stability of grid-connected DFIG wind farm. *IEEE Trans. Sustain. Energy* 2019, https://doi.org/10.1109/TSTE.2019.2897596
3. Yang B.; Yu T.; Shu H.; Dong J.; Jiang L. Robust sliding-mode control of wind energy conversion systems for optimal power extraction via nonlinear perturbation observers. *Appl. Energy* 2018, 210, 711–723.
4. Li Y.; Yang Z.; Li G.; Zhao D.; Tian W. Optimal Scheduling of an Isolated Microgrid With Battery Storage Considering Load and Renewable Generation Uncertainties. *IEEE Trans. Ind. Electron.* 2019, 66, 1565–1575.
5. Yang B.; Zhang X.; Yu T.; Shu H.; Fang Z. Grouped grey wolf optimizer for maximum power point tracking of doubly-fed induction generator based wind turbine. *Energy Convers. Manage.* 2017, 133, 427–443.
6. Jerin A.; Kaliannan P.; Subramaniam U.; Moursi M. Review on FRT solutions for improving transient stability in DFIG-WTs. *IET Renew. Power Gener.* 2018, 12, 1786–1799.

7. Gayen P.K.; Chatterjee D.; Goswami S.K. An improved low-voltage ride-through performance of DFIG based wind plant using stator dynamic composite fault current limiter. *ISA Trans*. 2016, 62, 333–348 https://doi.org/10.1016/j.isatra.2016.01.023 PMID: 26876377
8. Huang Q.; Zou X.; Zhu D.; Kang Y. Scaled current tracking control for doubly fed induction generator to ride-through serious grid faults. *IEEE Trans. Power Electron*. 2016, 31, 2150–2165.
9. Ahmed E.; Istvàn E. Short-circuit current reduction techniques of the doubly-fed induction generator based wind turbines for fault ride through enhancement. *IET Renew. Power Gener*. 2017, 11, 1033–1040.
10. Ghafouri M.; Karaagac U.; Karimi H.; Jensen S.; Mahseredjian J.; Faried S. An LQR Controller for Damping of Subsynchronous Interaction in DFIG-Based Wind Farms. *IEEE Trans. Power Syst*. 2017, 32, 4934–4942.
11. Jin P.; Li Y.; Li G.; Chen Z.; Zhai X. Optimized hierarchical power oscillations control for distributed generation under unbalanced conditions. *Appl. Energy* 2017, 194, 343–352.
12. Hazari M.R.; Mannan M.A.; Muyeen S.M.; Umemura A.; Takahashi R.; Tamura J. Stability Augmentation of a Grid-Connected Wind Farm by Fuzzy-Logic-Controlled DFIG-Based Wind Turbines. *Appl. Sci*. 2018, 8, 20–43.
13. Seyed A.; Zahra D.; Mohsen R.; Mohammad S. Model predictive fuzzy control for enhancing FRT capability of DFIG-based WT in real-time simulation environment. *Energy Syst*. 2018, 9, 899–919.
14. Zou X.; Zhu D.; Hu J.; Zhou S.; Kang Y. Mechanism Analysis of the Required Rotor Current and Voltage for DFIG-Based WTs to Ride-Through Severe Symmetrical Grid Faults. *IEEE Trans. Power Electron*. 2018, 33, 7300–7304.
15. Graham P.; Bashar Z.; David J.; Petros M. Evaluation of the Performance of a DC-Link Brake Chopper as a DFIG Low-Voltage Fault-Ride-Through Device. *IEEE Trans. Energy Conver*. 2013, 28, 535–542.
16. Seyed B.; Michael N.; Kashem M. A Modified DC Chopper for Limiting the Fault Current and Controlling the DC-Link Voltage to Enhance Fault Ride-Through Capability of Doubly-Fed Induction-Generator-Based Wind Turbine. *IEEE Trans. Ind. Appl*. 2019, 55, 2021–2032.
17. Sandro E.; Sidelmo M.; Braz J. Fault ride-through enhancement in DFIG with control of stator flux using minimised series voltage compensator. *IET Renew. Power Gener*. 2018, 12, 1234–1240.
18. Wessels C.; Gebhardt F.; Fuchs F. Fault ride-through of a DFIG wind turbine using a dynamic voltage restorer during symmetrical and asymmetrical grid faults. *IEEE Trans. Power Electron*. 2011, 26, 807–815.
19. Huang P.; Mohamed S.; Xiao W.; James L. Subsynchronous Resonance Mitigation for Series-Compensated DFIG-Based Wind Farm by Using Two-Degree-of-Freedom Control Strategy. *IEEE Trans. Power Syst*. 2015, 30, 1442–1454.
20. Rauf A.; Khadkikar V. An enhanced voltage Sag compensation scheme for dynamic voltage restorer. *IEEE Trans. Ind. Electron*. 2015, 62, 2683–2692.
21. Rini A.; Palanisamy K.; Sanjeevikumar P.; Umashankar S.; Vigna K. Improved Fault Ride Through Capability in DFIG Based Wind Turbines Using Dynamic Voltage Restorer With Combined Feed-Forward and Feed-Back Control. *IEEE Access* 2017, 5, 20494–20503.
22. Chen X.; Yan L.; Zhou X.; Sun H. A Novel DVR-ESS-Embedded Wind-Energy Conversion System. *IEEE Trans. Sustain. Energy* 2018, 9, 1265–1274.
23. Guo W.; Xiao L.; Dai S.; Xu X.; Li Y.; Wang Y. Evaluation of the performance of BTFCLS for enhancing LVRT capability of DFIG. *IEEE Trans. Power Electron*. 2015, 30, 3623–3637.
24. Rashid G.; Ali M. H. Transient Stability Enhancement of Doubly Fed Induction Machine-Based Wind Generator by Bridge-Type Fault Current Limiter. *IEEE Trans. Energy Convers*. 2015, 30, 939–947.
25. Rashid G.; Ali M. H. Nonlinear Control-Based Modified BFCL for LVRT Capacity Enhancement of DFIG-Based Wind Farm. *IEEE Trans. Energy Convers*. 2017, 32, 284–295.
26. Firouzi M.; Gharehpetian G. B. LVRT Performance Enhancement of DFIG-Based Wind Farms by Capacitive Bridge-Type Fault Current Limiter. *IEEE Trans. Sustain. Energy* 2018, 9, 1118–1125.
27. Chen L.; Deng C.; Zheng F.; Li S.; Liu Y.; Liao Y. Fault ride-through capability enhancement of DFIG-based wind turbine with a flux-coupling-type SFCL employed at different locations. *IEEE Trans. Appl. Supercond*. 2015, 25, Art. no. 5201505.
28. Chen L.; Zheng F.; Deng C.; Li Z.; Guo F. Fault ride-through capability improvement of DFIG-based wind turbine by employing a voltage-compensation-type active SFCL. *Can. J. Elect. Comput. Eng*. 2015, 38, 132–142.
29. Oliveira F.; Amorim A.; Encarnação L.; Fardin J.; Orlando M.; Silva S.; et al. Enhancing LVRT of DFIG by Using a Superconducting Current Limiter on Rotor Circuit. *Energies* 2016, 9, 16–27.

30. Zou Z.; Chen X.; Li C.; Xiao X.; Zhang Y. Conceptual design and evaluation of a resistive-type SFCL for efficient fault ride through in a DFIG. *IEEE Trans. Appl. Supercond.* 2016, 26, Art. no. 5600209.
31. Zou Z.; Xiao X.; Liu Y.; Zhang Y.; Wang Y. Integrated Protection of DFIG-Based Wind Turbine With a Resistive-Type SFCL Under Symmetrical and Asymmetrical Faults. *IEEE Trans. Appl. Supercond.* 2016, 26, Art. no. 5603005.
32. Hossain M.; Ali M. Transient stability improvement of doubly fed induction generator based variable speed wind generator using DC resistive fault current limiter. *IET Renew. Power Gener.* 2016, 10, 150–157.
33. Ou R.; Xiao X.; Zou Z.; Zhang Y.; Wang Y. Cooperative Control of SFCL and Reactive Power for Improving the Transient Voltage Stability of Grid-Connected Wind Farm With DFIGs. *IEEE Trans. Appl. Supercond.* 2016, 26, Art. no. 5402606.
34. Chen L.; Chen H.; Yang J.; He H.; Liu X.; Yu Y.; et al. Conceptual design and performance evaluation of a 35-kV/500-A flux-coupling-type SFCL for protection of a DFIG-based wind farm. *IEEE Trans. Appl. Supercond.* 2018, 28, Art. no. 5200607.
35. Du K.; Xiao X.; Wang Y.; Zheng Z.; Li C. Enhancing Fault Ride-Through Capability of DFIG-Based Wind Turbines Using Inductive SFCL With Coordinated Control. *IEEE Trans. Appl. Supercond.* 2019, 29, Art. no. 5400506.
36. Guo W.; Xiao L.; Dai S. Enhancing low-voltage ride-through capability and smoothing output power of DFIG with a superconducting fault-current limiter–magnetic energy storage system. *IEEE Trans. Energy Convers.* 2012, 27, 277–295.
37. Ngamroo I. Optimization of SMES-FCL for augmenting FRT performance and smoothing output power of grid-connected DFIG wind turbine. *IEEE Trans. Appl. Supercond.* 2016, 26, Art. no. 3800405.
38. Ngamroo I.; Karaipoom T. Cooperative control of SFCL and SMES for enhancing fault ride through capability and smoothing power fluctuation of DFIG wind farm. *IEEE Trans. Appl. Supercond.* 2014, 24, Art. no. 5400304.
39. Xiao X.; Yang R.; Chen X.; Zheng Z. Integrated DFIG protection with a modified SMES-FCL under symmetrical and asymmetrical faults. *IEEE Trans. Appl. Supercond.* 2018, 28, Art. no. 5400606.
40. Chen L.; Li G.; Chen H.; Tao Y.; Tian X.; Liu X.; et al. Combined Use of a Resistive SFCL and DC-link Regulation of a SMES for FRT Enhancement of a DFIG Wind Turbine Under Different Faults. *IEEE Trans. Appl. Supercond.* 2019, 29, Art. no. 5600408.
41. Morren J.; Sjoerd W. Short-Circuit Current of Wind Turbines With Doubly Fed Induction Generator. *IEEE Trans. Energy Convers.* 2007, 22, 174–180.
42. Ł H.; Moursi M.; Zeineldin H. A parallel capacitor control strategy for enhanced FRT capability of DFIG. *IEEE Trans. Sustain. Energy* 2015, 6, 303–312.
43. Naderi S.; Negnevitsky M.; Jalilian A.; Hagh M.; Muttaqi K. Low voltage ride-through enhancement of DFIG-based wind turbine using DC link switchable resistive type fault current limiter. *Int. J. Elect. Power* 2017, 86, 104–119.
44. Yang L.; Xu Z.; Ostergaard J.; Dong Z.; Wong K. Advanced control strategy of DFIG wind turbines for power system fault ride through. *IEEE Trans. Power Syst.* 2012, 27, 713–722.
45. Shi J.; Tang Y.; Yang K.; Chen L.; Ren L.; Li J.; et al. SMES Based Dynamic Voltage Restorer for Voltage Fluctuations Compensation. *IEEE Trans. Appl. Supercond.* 2010, 20, 1360–1364.
46. Ajaei F.; Afsharnia S.; Kahrobaeian A.; Farhangi S. A Fast and Effective Control Scheme for the Dynamic Voltage Restorer. *IEEE Trans. Power Del.* 2011, 26, 2398–2406.
47. Ouyang J.; Xiong X. Characteristics of short-circuit current of wind turbine driven DFIG and its impacts on the grid-connected distribution network. *Automat. Electric Power Syst.* 2010, 34, 106–110.
48. Chen L.; Li Z.; Deng C.; Liu H.; Weng Y.; Xu Q.; et al. Effects of a flux-coupling type superconducting fault current limiter on the surge current caused by closed-loop operation in a 10kV distribution network. *Int. J. Elect. Power Energy Syst.* 2015, 69, 160–166.
49. Chen L.; Pan H.; Deng C.; Zheng F.; Li Z.; Guo F. Study on the Application of a Flux-Coupling-Type Superconducting Fault Current Limiter for Decreasing HVdc Commutation Failure. *Can. J. Elect. Comput. Eng.* 2015, 38, 10–19.
50. Abad G.; López J.; Rodríguez M.; Marroyo L.; Iwanski G. Doubly Fed Induction Machine: Modeling and Control for Wind Energy Generation. Hoboken, NJ, USA: Wiley, 2011.
51. Ling Y.; Cai X.; Wang N. Rotor current transient analysis of DFIG-based wind turbines during symmetrical voltage faults. *Energy Convers. Manag.* 2013, 76, 910–917.
52. Chen L.; Chen H.; Yang J.; Zhu L.; Tang Y.; Koh L.; et al. Comparison of Superconducting Fault Current Limiter and Dynamic Voltage Restorer for LVRT Improvement of High Penetration Microgrid. *IEEE Trans. Appl. Supercond.* 2017, 27, Art. no. 3800607.

53. Xiang D.; Ran L.; Tavner P.; Yang S. Control of a doubly fed induction generator in a wind turbine during grid fault ride-through. *IEEE Trans. Energy Convers.* 2006, 21, 652–662.

54. Rahimi M.; Parniani M. Transient performance improvement of wind turbines with doubly fed induction generators using nonlinear control strategy. *IEEE Trans. Energy Convers.* 2010, 25, 514–525.

55. Rahmann C.; Haubrich H.; Moser A.; Palma-Behnke R.; Vargas L.; Salles M. Justified Fault-Ride-Through Requirements for Wind Turbines in Power Systems. *IEEE Trans. Power Syst.* 2011, 26, 1555–1563.

56. Xu S.; Lu Y.; Wang Y. A Section Voltage Based Inverse Timing Protection Method for Microgrid. *Automat. Electric Power Syst.* 2014, 38, 68–73.

57. Tohidi S.; Tavner P.; McMahon R.; Oraee H.; Zolghadri M.; Shao S.; et al. Low voltage ride-through of DFIG and brushless DFIG: Similarities and differences. *Elect. Power Syst. Res.* 2014, 110, 64–72.